Master's Thesis of Engineering

Surface modification of $LiNi_{0.945}Co_{0.04}Al_{0.015}O_2$ with phosphono compounds for safe Li ion Batteries

고안정성 리튬이온전지를 위한 포스포노 화합물을 이용한 $LiNi_{0.945}Co_{0.04}Al_{0.015}O_2$의 표면 개질

2022년 8월

서울대학교 대학원

화학생물공학부

정해민

Surface modification of $LiNi_{0.945}Co_{0.04}Al_{0.015}O_2$ with phosphono compounds for safe Li ion Batteries

Advisor Kyu Tae Lee

Submitting a master's thesis of
engineering

August 2022

Graduate School of Chemical and Biological Engineering
Seoul National University
Chemical and Biological Engineering

Haemin Jeong

Confirming the master's thesis written by
Haemin Jeong
August 2022

Chair	Nam, Jaewook	(Seal)
Vice Chair	Lee, Kyu Tae	(Seal)
Examiner	Lee, Changha	(Seal)

Abstract

Ni-rich layered oxide is considered as a promising cathode materials, owing to its high practical capacity. As the content of nickel increases, the capacity of these materials increases but structural stability decreases at the same time.

Structural instability of such oxygen-containing cathodes can lead to release of the cathode lattice oxygen in form of O_2•. Oxygen release leads to severe degradation of the cathode performance and deteriorates the safety of the battery by triggering a thermal runaway.

In this paper, to improve thermal stability, PBA-coated NCA is introduced to suppress the evolution of oxygen radicals because the radical- scavenging coating layer captures oxygen radicals evolved from cathode lattice structure.

Radical - scavenging coating layer is obtained through surface engineering using phosphono benzoic acid, containing phosphorus which is known to scavenge free radicals. These surface modifications lead to improved thermal stability and diminished electrolyte decomposition and gas evolution, exhibiting similar electrochemical performance.

Keyword : Lithium ion batteries, Ni-rich Cathode, thermal stability, radical scavenging, oxygen evolution, battery safety

Student Number : 2020-29311

Table of Contents

List of Figures

Figure 12. (a) Voltage profiles of bare and 0.5 wt% PBA- coated $LiNi_{0.945}Co_{0.04}Al_{0.01.5}O_2$ electrodes. (b) Cycle performances of bare and 0.5 wt% PBA-coated $LiNi_{0.945}Co_{0.04}Al_{0.01.5}O_2$ electrodes at a 0.5 C rate (100 mA g^{-1}).

Chapter 1. Introduction

1.1. Study Background

Recently, Lithium-ion batteries have been required for higher energy density. [1-5] Ni-rich layered oxides, LiNixCoyMnzO2 (NCM) and LiNixCoyAlzO2 (NCA) with x + y + z = 1 and x >= 0.8, have recently been investigated as cathode materials for high energy density Li-ion batteries due to their comprehensive advantages in terms of theoretical capacity, working potential and manufacture cost. [6-9] The demand for higher energy density makes Ni content higher, which increases specific capacity but decreases thermal stability. [10-15] For this reason, research about thermal stability of cathode should be accompanied with energy density. [16-19]

This is attributed that the lattice oxygen becomes vulnerable with increasing the lithium extraction from the crystalline structure. Structural instability of such oxygen-containing cathodes can lead to release of the cathode lattice oxygen in form of O2•. [20-23] Oxygen release leads not to severe degradation of the cathode performance and deteriorates the safety of the battery by triggering

a thermal runaway and generating flammable gas. [24−26]

For this reason, many studies were focused on the development of cathode materials for LIBs. For example, cation doping for stabilization of lattice structure, nonflammable electrolytes and oxygen scavenging additives for preventing the propagation of oxygen radicals has been investigated. [27−35]

1.2. Purpose of Research

To improve thermal stability, scavenging oxygen radicals is essential for Ni-rich cathode materials. For this reason, we obtained surface-modified Ni-rich cathode materials to scavenge oxygen radicals released from charged cathode. We chose phosphono benzoic acid, containing phosphono functional group that is widely known to scavenge free radicals. PBA-coated $LiNi_{0.945}Co_{0.04}Al_{0.015}O_2$ suppressed the evolution of oxygen radicals from charged cathode, resulting in a reduced gas generation and improved thermal stability without sacrificing electrochemical performance compared to the bare $LiNi_{0.945}Co_{0.04}Al_{0.015}O_2$.

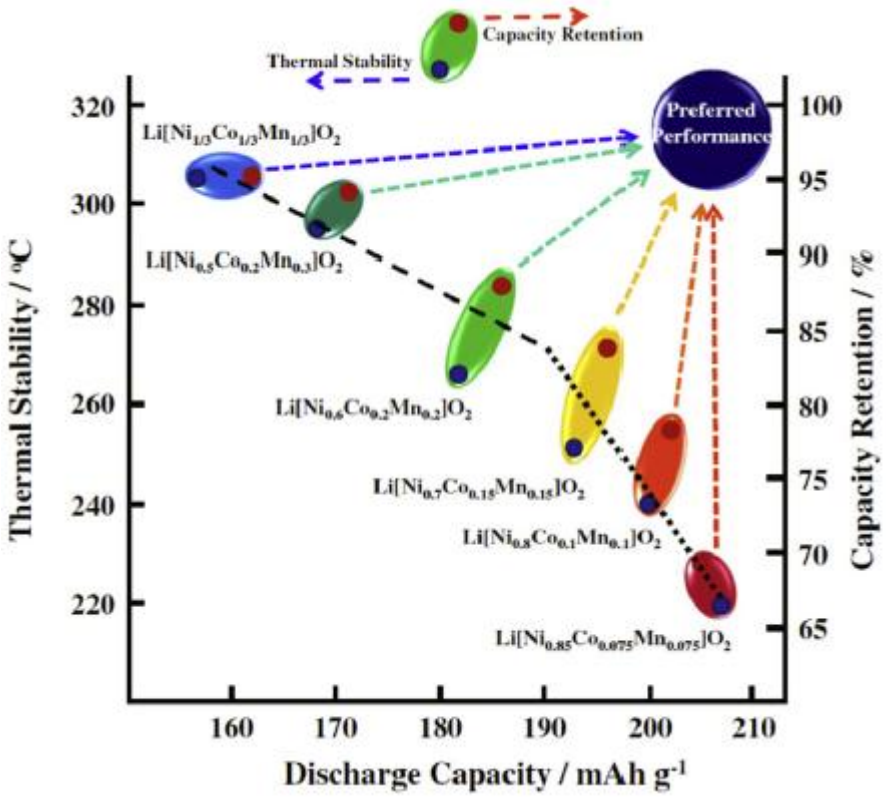

Figure 1. Fundamental characteristics of NCM materials. Schematic correlation of performance and safety with Ni content

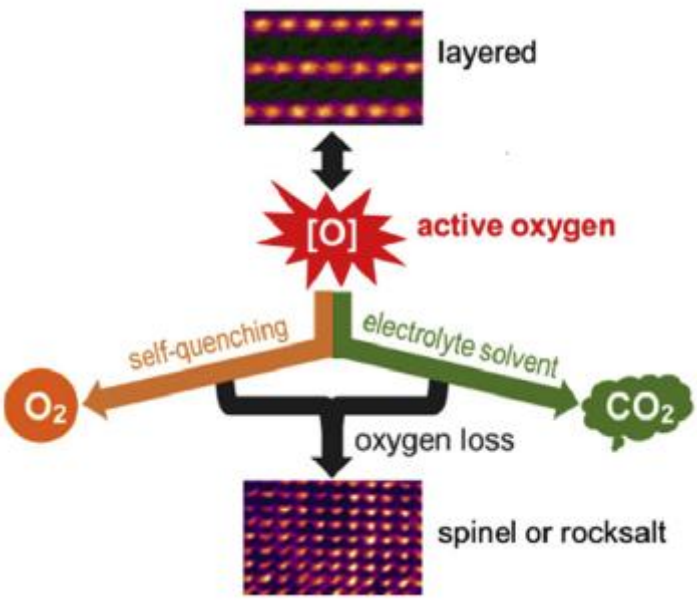

Figure 2. Schematic illustration of Oxygen evolution and resultant gas generation and layered–spinel–rock salt phase transition

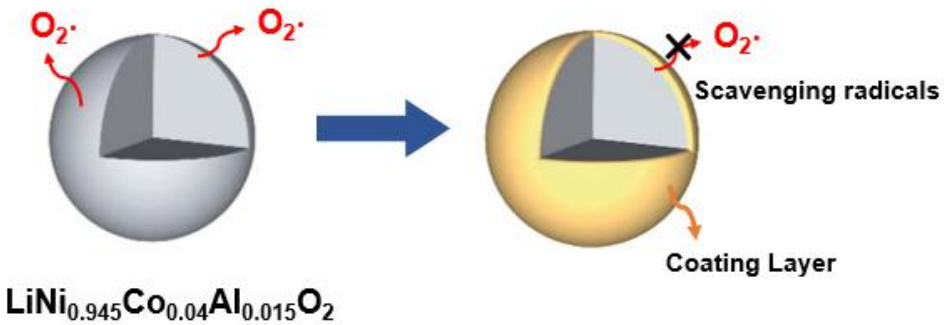

Figure 3. Schematic concept of radical-scavenging coating layer

Chapter 2. Experimental section

2.1. Synthesis

To obtain PBA-coated NCA, $LiNi_{0.945}Co_{0.04}Al_{0.015}O_2$ (Samsung SDI, Korea) and Phosphono benzoic acid were immersed into acetonitrile (anhydrous, 99.8%, Sigma-aldrich). Citric acid was added to the mixture as a catalyst and mixed at 80℃. The product was obtained and dried in vacuum at room temperature.

2.2. Material characterization

X-ray diffraction(XRD) patterns of powders were acquired using a D2 phaser with Cu-Kα radiation (λ=1.5148Å) operated in the 2θ range of 10° -80° . Thermogravimetric analysis was carried out with a simultaneous DTA/TGA analyzer (TA instrument, DTA) under an air atmosphere with a heating rate of 10℃/min. Fourier-transform infrared spectroscopy (FT-IR) was performed using a FT-IR spectrometer (Bruker, TENSOR27). Scanning electron microscopy (SEM) analysis was carried out using a field emission scanning electronic microscope (Carl Zeiss, Auriga). Transmission electron microscopy (TEM) images were obtained using a Cs-corrected scanning transmission electron microscope (JEOL Ltd., JEM-ARM200F). Cross-sectional TEM specimens were prepared with a FIB system after samples were coated with carbon and platinum. Electron Paramagnetic Resonance (EPR) analysis was carried out at room temperature on a Bruker EMX Micro spectrometer. The thermal stability of the charge cathodes was conducted by DSC (TA instrument, DSC25) measurements.

2.3. Differential electrochemical mass spectrometry

Differential electrochemical mass spectrometry was conducted using an HPR-20 R&D benchtop gas analysis system (Hiden analyrical, UK) and a WBCS-3000 (WonA Tech. Korea). Electrochemical cells were assembled using airtight home-made Swagelok cells under Ar atmosphere. The diameters of the working electrode ($LiNi_{0.945}Co_{0.04}Al_{0.015}O_2$) and the counter electrode (Li metal) were 9mm and 11mm, respectively. An excess amount of electrolyte (100 μL), which was 1M $LiPF_6$ in ethylene carbonate (EC) : diethyl carbonate (DEC) (1:1 volume ratio, Soulbrain Co.Ltd.) owing to its much lower volatility, was used to prevent the cells from drying out until the end of the experiment. The cell connected to the battery cycler was continuously purged with He gas at a constant flow rate of 14.3mL min^{-1}. Exhaust gas from the cell was fed to the inlet of the gas analyzer. To sufficiently remove O_2 leaked in during the cell connection, a charging current (20mA g^{-1}) was applied after 24 hours of He purging.

2.4. Electrochemical characterization

$LiNi_{0.945}Co_{0.04}Al_{0.015}O_2$ powders were mixed with carbon black (Super P) and polyvinylidene fluoride (PVDF) in a weight ratio of 8:1:1. The slurry was casted onto an Al foil current collector. The electrodes were dried at 120℃ for overnight in a vacuum oven. The mass loading of active materials was 2.3−2.5 mg cm^{-2}. The electrochemical performance of $LiNi_{0.945}Co_{0.04}Al_{0.015}O_2$ was evaluated in a voltage range 2.7−4.3 V vs. Li/Li^+ at a 0.5 C rate (100 mA g^{-1}) after a formation cycle at 0.1 C rate. Galvanostatic experiments were carried out using 2032 coin cells with a Li metal and 1.3M $LiPF_6$ in ethylene carbonate (EC) : ethylmethyl carbonate (EMC) : dimethyl carbonate (DMC) (3:4:3 volume ratio, Soulbrain Co. Ltd.) at 30℃.

Chapter 3. Results and discussion

3.1. PBA coating on NCA

The XRD patterns of $LiNi_{0.945}Co_{0.04}Al_{0.015}O_2$ powders show that $LiNi_{0.945}Co_{0.04}Al_{0.015}O_2$ has the O3-type hexagonal α-NaFeO2 structure (space group: R3m) (Figure 4a). Figure 4b shows the Thermogravimetric analysis (TGA) profiles in the temperature range between 30℃ and 600℃. This indicates a significant weight loss of around 0.5 wt% and 1 wt%. The IR spectra of bare and 0.5 wt% PBA-coated $LiNi_{0.945}Co_{0.04}Al_{0.015}O_2$ reveals that the characteristic IR bands of PBA were observed in the IR spectrum of 4 wt% PBA-coated $LiNi_{0.945}Co_{0.04}Al_{0.015}O_2$, which was coated with excessive PBA to confirm the functional group clearly (Figure 5). This implies that PBA layer was coated on the $LiNi_{0.945}Co_{0.04}Al_{0.015}O_2$ surfaces. This is also supported by the SEM images of 0.5 wt% and 1 wt% PBA-coated $LiNi_{0.945}Co_{0.04}Al_{0.015}O_2$ particles (Figure 6), unlike bare $LiNi_{0.945}Co_{0.04}Al_{0.015}O_2$ that has clean surfaces. This is also supported by the cross-sectional STEM and EDS mapping images of 0.5 wt% PBA-coated

$LiNi_{0.945}Co_{0.04}Al_{0.015}O_2$. Figure 7a shows the cross-sectional scanning transmission electron microscopy (STEM) and the corresponding energy dispersive X-ray spectroscopy (EDS) mapping images of 0.5 wt% PBA-coated $LiNi_{0.945}Co_{0.04}Al_{0.015}O_2$. Cross-sectional STEM specimens were obtained using a focused ion beam (FIB) system. The STEM image show that a thin layer was uniformly coated on the $LiNi_{0.945}Co_{0.04}Al_{0.015}O_2$ surface. P atoms were observed in the thin coating layer, as shown in the corresponding EDS mapping image. This implies that the thin coating layer is PBA because PBA contains P atoms. In addition, Figure 7b displays the EDS line profiles of Ni and P atoms near the $LiNi_{0.945}Co_{0.04}Al_{0.015}O_2$ surface to estimate the thickness of PBA coating layers were approximately 20nm for 0.5 wt% PBA-coated $LiNi_{0.945}Co_{0.04}Al_{0.015}O_2$ particles.

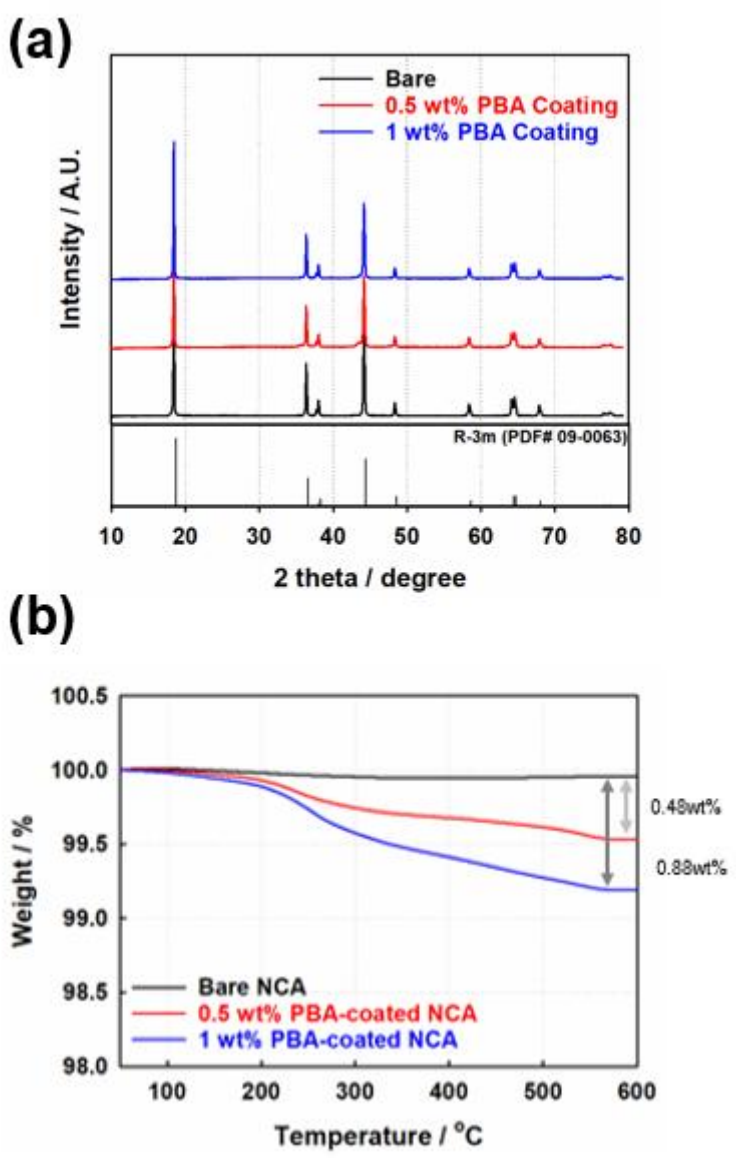

Figure 4. (a) XRD patterns and (b) TGA profiles

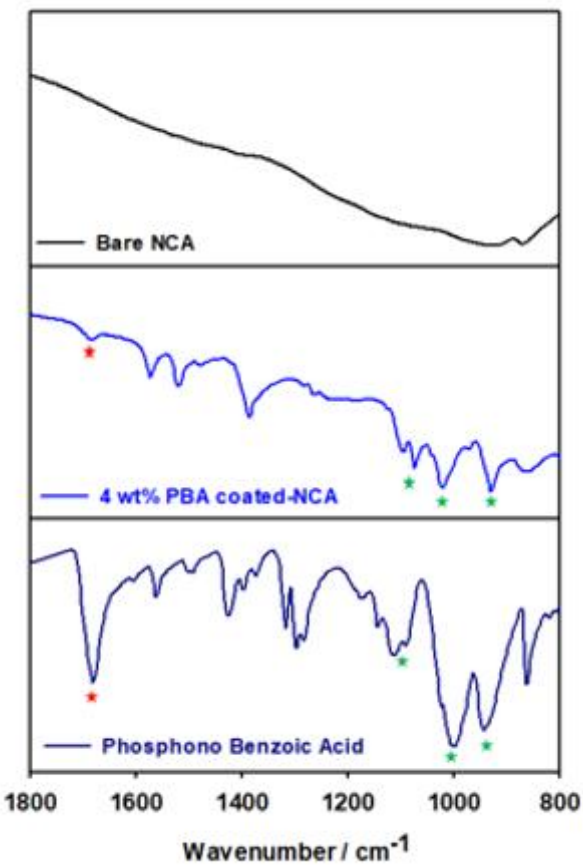

Figure 5. FT-IR spectra of bare NCA and 4 wt% PBA-coated NCA and Phosphono benzoic acid

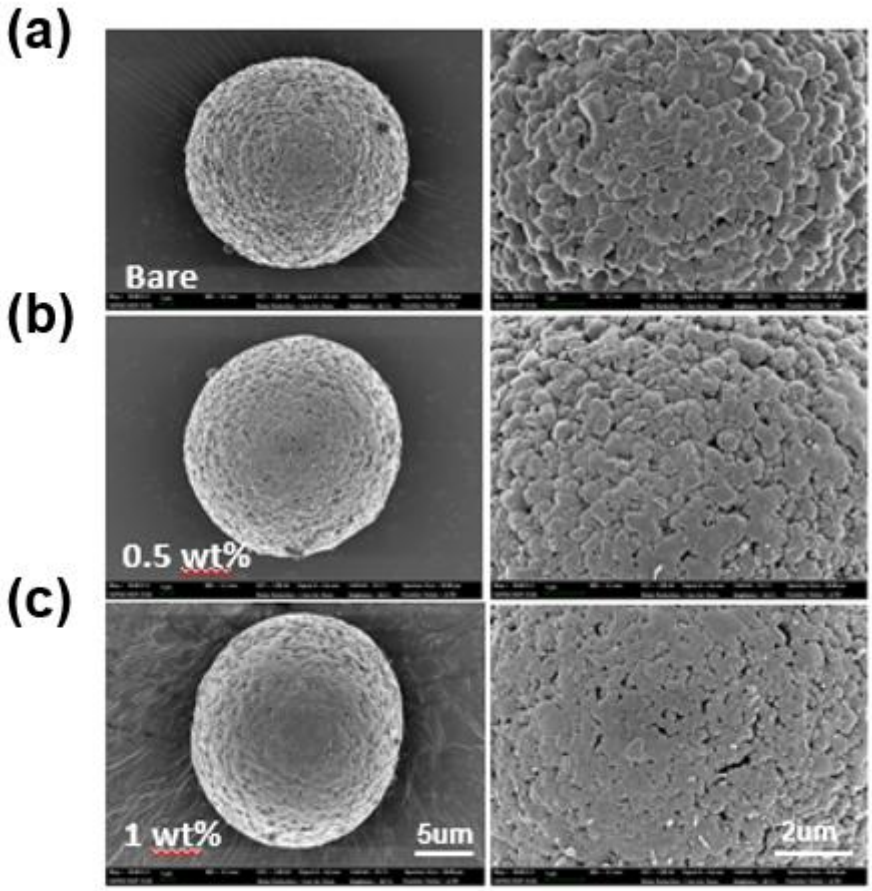

Figure 6. SEM images of (a) bare, (b) 0.5 wt% PBA-coated and (c) 1 wt% PBA-coated NCA powders

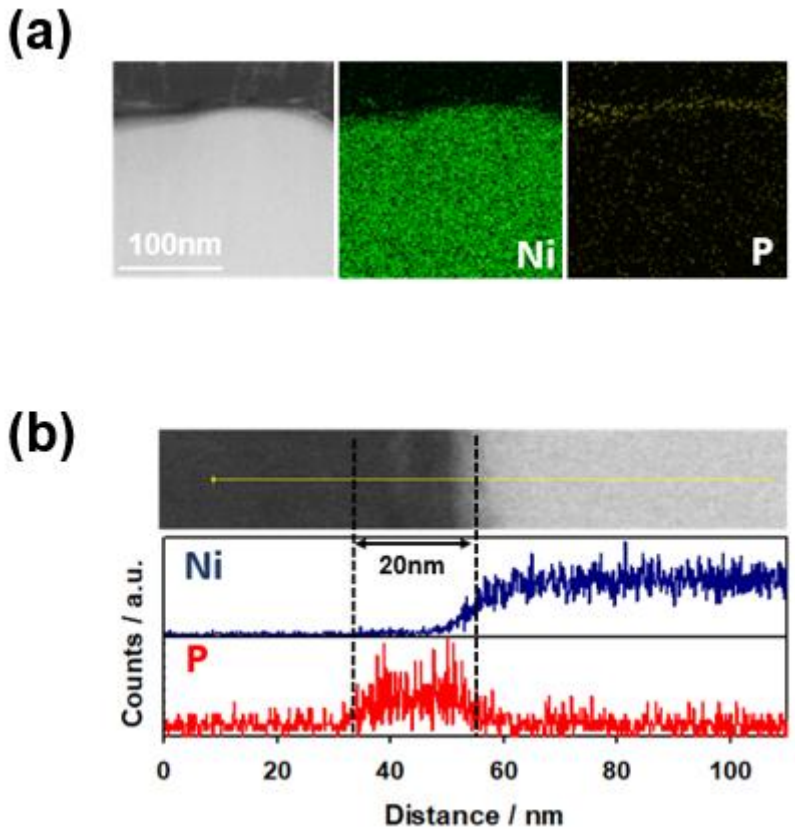

Figure 7. (a) Cross-sectional STEM and EDS mapping images of 1 wt% PBA-coated NCA. (b) EDS line profiles of 1 wt% PBA-coated NCA powders

3.2. Effect of scavenging radicals

EPR was employed to investigate the free radicals generated between the fully charged $LiNi_{0.945}Co_{0.04}Al_{0.015}O_2$ cathode and the electrolyte solvent.

Figure 8a shows that EPR spectra of electrolyte in which charged cathode after 1 cycle was immersed. It can be seen that there is a peak of bare electrode. This suggests that reactive oxygen radicals released at the charged cathode surface attack electrolyte molecules and generate organic radicals. In the case of 0.5 wt% PBA-coated $LiNi_{0.945}Co_{0.04}Al_{0.015}O_2$, however, there is no signal of radicals in PBA-electrolyte. This implies that the amount of free radicals of PBA-electrolyte was significantly small compared to the bare-electrolyte. Figure 8b shows that EPR spectra of electrolyte in which charge cathode after 100 cycle was immersed. It can be also seen that there is a peak of bare electrode, more strongly. This suggests that lattice structure of cycled electrode was more unstable, which released more oxygen radicals when immersed in electrolyte. In the case of PBA-coated $LiNi_{0.945}Co_{0.04}Al_{0.015}O_2$, EPR signals become weaker with increased amount of PBA in coated NCA, which shows the radical-scavenging effect of PBA. This suggests that evolved oxygen radicals were captured by the PBA on

the cathode surface and the side reactions at the cathode–electrolyte interface were suppressed.

The differential scanning calorimetry (DSC) analysis was performed to evaluate the ability to scavenge oxygen radicals and to evaluate the thermal decomposition behavior of $LiNi_{0.945}Co_{0.04}Al_{0.015}O_2$ in the presence of an electrolyte. The heat flow of the cathode material charged to 4.3V with electrolyte is shown in Figure 9. Each exothermic peak in the DSC curves was observed during the heating process. It showed that the exothermic peak of bare $LiNi_{0.945}Co_{0.04}Al_{0.015}O_2$ appears at 208℃, which is due to the electrolyte combustion caused by oxygen release from the active cathode material.

In the case of PBA–coated $LiNi_{0.945}Co_{0.04}Al_{0.015}O_2$, the exothermic peak temperature becomes higher with drastically reduced heat release. The peak temperature of the exothermic reaction was 224℃ for the 0.5 wt% PBA–coated $LiNi_{0.945}Co_{0.04}Al_{0.015}O_2$ and 231℃ for the 1 wt% PBA–coated $LiNi_{0.945}Co_{0.04}Al_{0.015}O_2$. This is attributed that PBA at the cathode surface acted as a radical scavenger during thermal decomposition of $LiNi_{0.945}Co_{0.04}Al_{0.015}O_2$ in the presence of an electrolyte. This implies that the release of oxygen is inhibited

by the surface modification of PBA.

The scavenging property of PBA-coated $LiNi_{0.945}Co_{0.04}Al_{0.015}O_2$ could be further confirmed by Differential Electrochemical Mass Spectrometry (DEMS). DEMS was performed to monitor the gas evolution during charging process, using a low volatility electrolyte in order to obtain accurate gas evolution data. Figure 10 shows that the O_2 and CO_2 gas evolution was monitored in the DEMS measurement during the first charging process up to 4.8V of the bare $LiNi_{0.945}Co_{0.04}Al_{0.015}O_2$ electrode and 1 wt% PBA-coated $LiNi_{0.945}Co_{0.04}Al_{0.015}O_2$ electrode, respectively. O2 gas evolution is hardly observed in both bare NCA electrode and 1 wt% PBA-coated $LiNi_{0.945}Co_{0.04}Al_{0.015}O_2$ electrode. However, CO_2 gas evolution is significantly lower in 1 wt% PBA-coated $LiNi_{0.945}Co_{0.04}Al_{0.015}O_2$ electrode. The CO_2 evolution was resulted from the chemical oxidization of the electrolyte by the oxygen radicals that were released from the $LiNi_{0.945}Co_{0.04}Al_{0.015}O_2$. Therefore, this suggests that chemical oxidization of the electrolyte by the oxygen radicals decreased in 1 wt% PBA-coated $LiNi_{0.945}Co_{0.04}Al_{0.015}O_2$ electrode. This implies that PBA coated on $LiNi_{0.945}Co_{0.04}Al_{0.015}O_2$ cathode suppressed the decomposition of electrolyte effectively.

To support the DEMS results, we performed XPS analysis to examine the components of organic CEI, which can be triggered by reaction with oxygen radicals. The Figure 11 shows the O 1s and F 1s spectra for the bare $LiNi_{0.945}Co_{0.04}Al_{0.015}O_2$ and PBA-coated $LiNi_{0.945}Co_{0.04}Al_{0.015}O_2$. The lattice oxygen peak at 529.5 eV is higher in intensity for the cycled PBA-coated $LiNi_{0.945}Co_{0.04}Al_{0.015}O_2$ electrode compared to the cycled bare $LiNi_{0.945}Co_{0.04}Al_{0.015}O_2$ electrode. This indicates that the cycled PBA-coated electrode has a thinner CEI on the cathode, as compared to cycled bare $LiNi_{0.945}Co_{0.04}Al_{0.015}O_2$ electrode. This implies that carbonate electrolyte decomposition by oxygen radicals decreased at the PBA-coated $LiNi_{0.945}Co_{0.04}Al_{0.015}O_2$ electrode. Therefore, the XPS result revealed that the reduction in gas evolution is due to the radical scavenging ability of PBA.

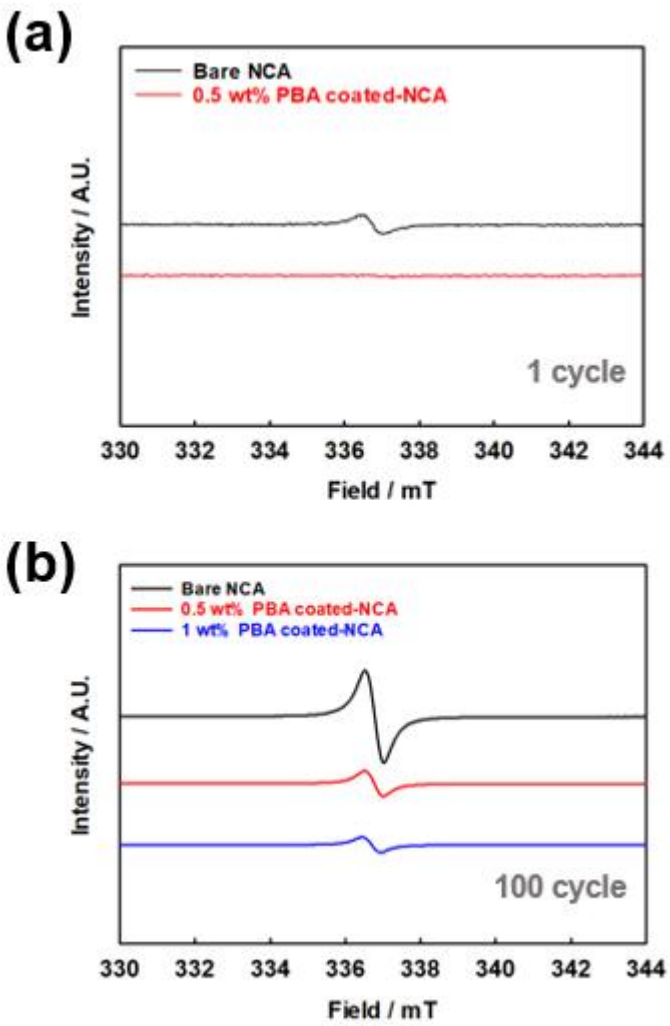

Figure 8. EPR spectra of electrolyte after storage with cathode at a charged state subjected to 4.3V

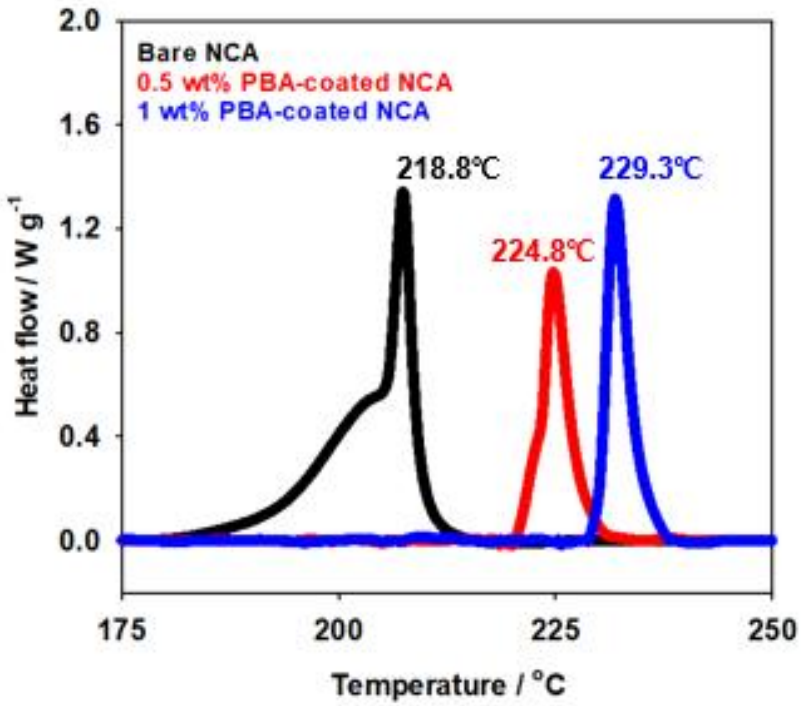

Figure 9. DSC profiles of NCA cathode charged to 4.3V

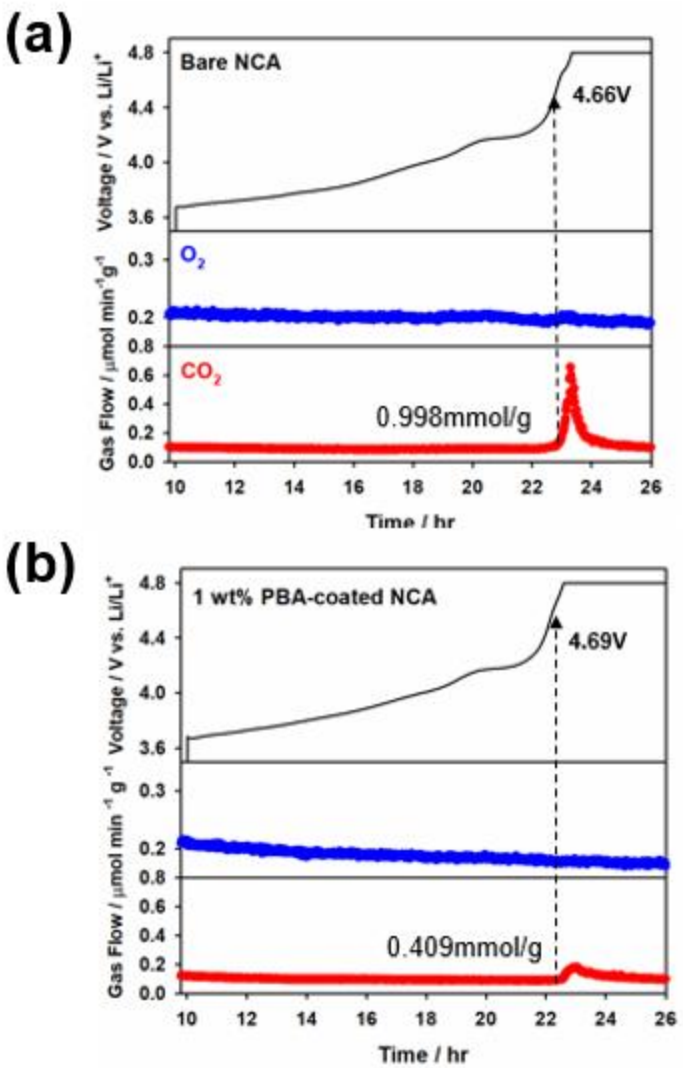

Figure 10. Differential electrochemical mass spectrometry (DEMS) spectra of a) Bare NCA and b) 1 wt% PBA-coated NCA electrodes when charged to 4.8V at 0.1C current density.

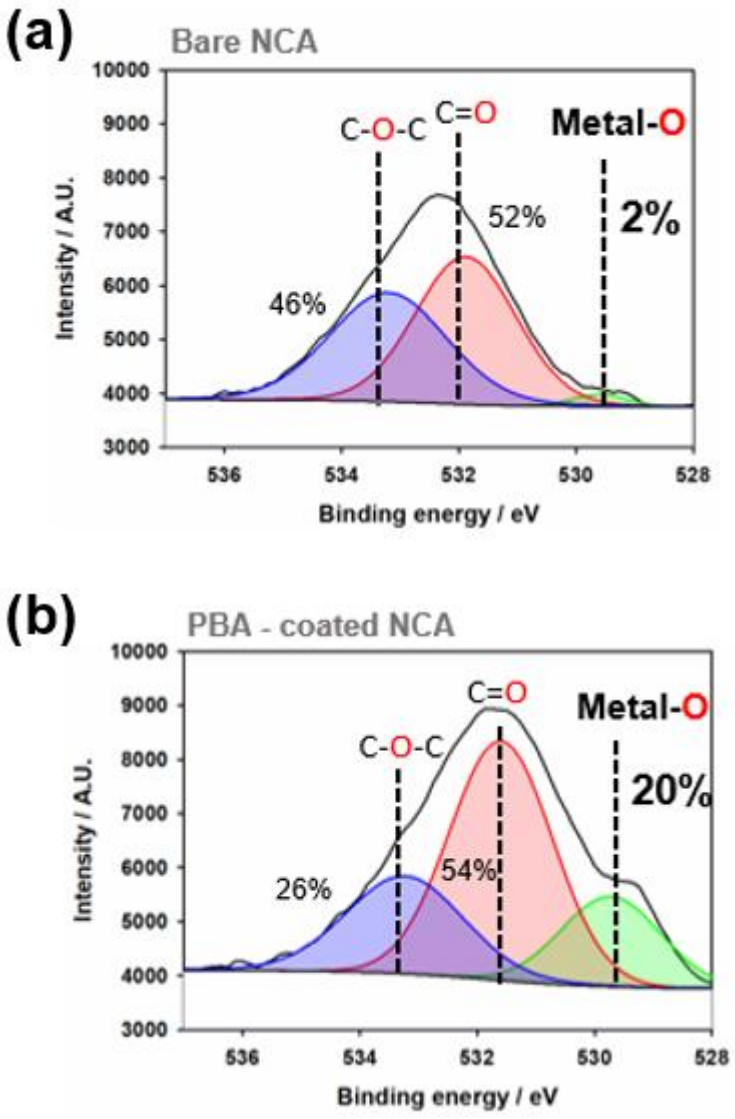

Figure 11. O 1s XPS surface component analysis of bare and 1 wt% PBA – coated NCA electrode after first charging.

3.3. Electrochemical performances

We compared the electrochemical performances of bare and 0.5 wt% PBA-coated $LiNi_{0.945}Co_{0.04}Al_{0.015}O_2$ electrodes at 30℃. Figure 12 shows the voltage profiles and cycle performance of bare and 0.5 wt% PBA-coated $LiNi_{0.945}Co_{0.04}Al_{0.015}O_2$ electrodes. The bare NCA electrode delivered a reversible capacity of 208mAh/g and 0.5 wt% PBA-coated $LiNi_{0.945}Co_{0.04}Al_{0.015}O_2$ electrode delivered a reversible capacity of 204mAh/g, which is reduced initial reversible capacity. This is attributed to the fact that PBA coating layer increased cell impedance during cycling.

We observed reduced initial reversible capacity and a little poorer cycle performance of PBA-coated $LiNi_{0.945}Co_{0.04}Al_{0.015}O_2$ electrode. However, at that time, PBA coating layer is beneficial for suppressing the irreversible electrolyte decomposition at high voltages, resulting in similar electrochemical performances compared with bare $LiNi_{0.945}Co_{0.04}Al_{0.015}O_2$.

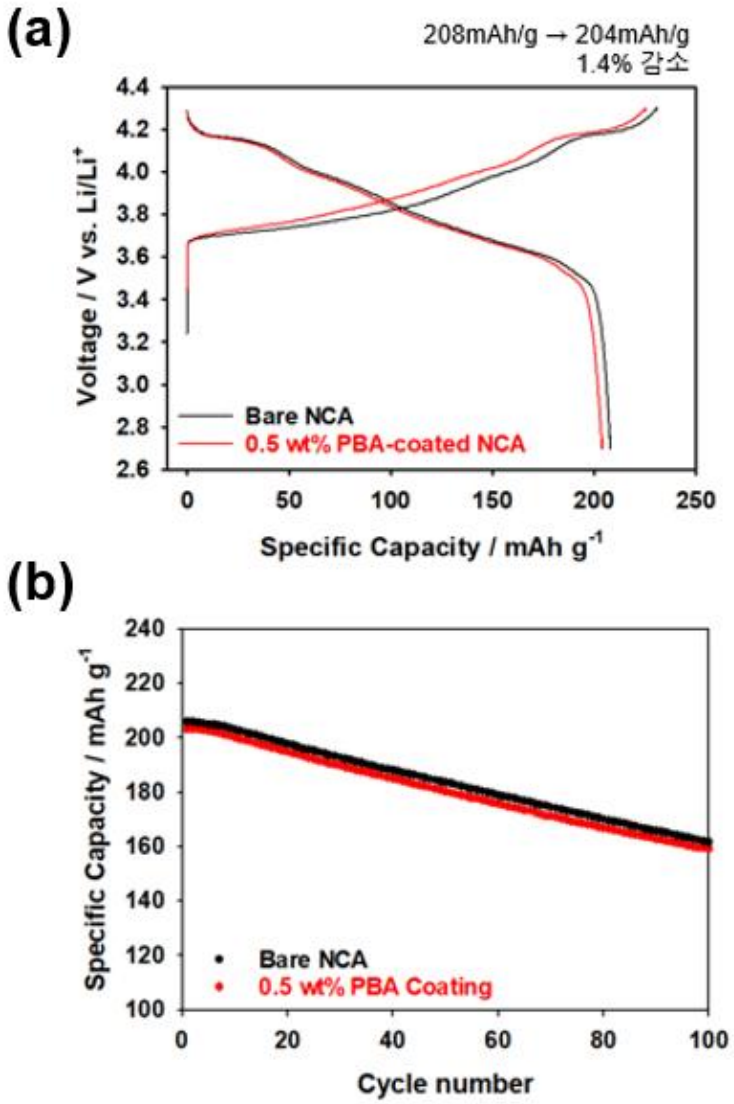

Figure 12. (a) Voltage profiles of bare and 0.5 wt% PBA- coated $LiNi_{0.945}Co_{0.04}Al_{0.01.5}O_2$ electrodes. (b) Cycle performances of bare and 0.5 wt% PBA-coated $LiNi_{0.945}Co_{0.04}Al_{0.01.5}O_2$ electrodes at a 0.5 C rate (100 mA g^{-1}).

Chapter 4. Conclusion

In this research, we introduced radical – scavenging Ni-rich cathode for Li ion batteries. We obtained radical – scavenging Ni-rich cathode using phosphono benzoic acid, known as an effective radical scavenger. By means of TGA, FT-IR, STEM and EDS, we demonstrated that PBA was coated on the $LiNi_{0.945}Co_{0.04}Al_{0.015}O_2$ surface through Fisher-esterification. Characterization using EPR analysis confirmed that the PBA-coated $LiNi_{0.945}Co_{0.04}Al_{0.015}O_2$ suppressed oxygen radical evolution from cathode and prevented the propagation of oxygen radicals. The DEMS analysis showed reduced CO_2 gas evolution at high voltages for the PBA-coated $LiNi_{0.945}Co_{0.04}Al_{0.015}O_2$ electrode, demonstrating radical – scavenging effects of PBA coating layer. We also demonstrated, by means of XPS, the role of PBA coating layer in the DEMS analysis was scavenging oxygen radicals. DSC analysis also revealed that PBA-coated $LiNi_{0.945}Co_{0.04}Al_{0.015}O_2$ exhibits improved thermal stability compared to bare $LiNi_{0.945}Co_{0.04}Al_{0.015}O_2$ electrode, which suggests the improved safety of cathode. Finally, electrochemical performances maintain similar capacity and cycle performances. These data allow us to conclude that the improved thermal stability and similar electrochemical performances, These findings provide

surface engineering insights into strategies to improve thermal stability of Ni-rich cathode for Li-ion batteries.

References

1. Myung, S. T.; Maglia, F.; Park, K. J.; Yoon, C. S.; Lamp, P.; Kim, S. J.; Sun, Y. K. Nickel-Rich Layered Cathode Materials for Automotive Lithium-Ion Batteries: Achievements and Perspectives. *Acs Energy Lett* 2017, *2* (1), 196-223. DOI: 10.1021/acsenergylett.6b00594.
2. Goodenough, J. B.; Park, K. S. The Li-Ion Rechargeable Battery: A Perspective. *J Am Chem Soc* 2013, *135* (4), 1167-1176. DOI: 10.1021/ja3091438.
3. Manthiram, A.; Knight, J. C.; Myung, S. T.; Oh, S. M.; Sun, Y. K. Nickel-Rich and Lithium-Rich Layered Oxide Cathodes: Progress and Perspectives. *Adv Energy Mater* 2016, *6* (1). DOI: 10.1002/aenm.201501010.
4. Lu, J.; Chen, Z. H.; Ma, Z. F.; Pan, F.; Curtiss, L. A.; Amine, K. The role of nanotechnology in the development of battery materials for electric vehicles. *Nat Nanotechnol* 2016, *11* (12), 1031-1038. DOI: 10.1038/nnano.2016.207.
5. Zou, L. F.; Zhao, W. G.; Liu, Z. Y.; Jia, H. P.; Zheng, J. M.; Wang, G. F.; Yang, Y.; Zhang, J. G.; Wang, C. M. Revealing Cycling Rate-Dependent Structure Evolution in Ni-Rich Layered Cathode Materials. *Acs Energy Lett* 2018, *3* (10), 2433-2440. DOI: 10.1021/acsenergylett.8b01490.
6. de Biasi, L.; Schiele, A.; Roca-Ayats, M.; Garcia, G.; Brezesinski, T.; Hartmann, P.; Janek, J. Phase Transformation Behavior and Stability of LiNiO2 Cathode Material for Li-Ion Batteries Obtained from InSitu Gas Analysis and Operando X-Ray Diffraction. *Chemsuschem* 2019, *12* (10), 2240-2250. DOI: 10.1002/cssc.201900032.
7. Li, T. Y.; Yuan, X. Z.; Zhang, L.; Song, D. T.; Shi, K. Y.; Bock, C. Degradation Mechanisms and Mitigation Strategies of Nickel-Rich

NMC-Based Lithium-Ion Batteries. *Electrochem Energy R* 2020, *3* (1), 43-80. DOI: 10.1007/s41918-019-00053-3.

8. Manthiram, A.; Song, B. H.; Li, W. D. A perspective on nickel-rich layered oxide cathodes for lithium-ion batteries. *Energy Storage Mater* 2017, *6*, 125-139. DOI: 10.1016/j.ensm.2016.10.007.
9. Liu, W.; Oh, P.; Liu, X.; Lee, M. J.; Cho, W.; Chae, S.; Kim, Y.; Cho, J. Nickel-Rich Layered Lithium Transition-Metal Oxide for High-Energy Lithium-Ion Batteries. *Angew Chem Int Edit* 2015, *54* (15), 4440-4457. DOI: 10.1002/anie.201409262.
10. Liu, K.; Liu, Y. Y.; Lin, D. C.; Pei, A.; Cui, Y. Materials for lithium-ion battery safety. *Sci Adv* 2018, *4* (6). DOI: 10.1126/sciadv.aas9820.
11. Feng, X. N.; Ouyang, M. G.; Liu, X.; Lu, L. G.; Xia, Y.; He, X. M. Thermal runaway mechanism of lithium ion battery for electric vehicles: A review. *Energy Storage Mater* 2018, *10*, 246-267. DOI: 10.1016/j.ensm.2017.05.013.
12. Huang, Y.; Lin, Y. C.; Jenkins, D. M.; Chernova, N. A.; Chung, Y.; Radhakrishnan, B.; Chu, I. H.; Fang, J.; Wang, Q.; Omenya, F.; et al. Thermal Stability and Reactivity of Cathode Materials for Li-Ion Batteries. *Acs Appl Mater Inter* 2016, *8* (11), 7013-7021. DOI: 10.1021/acsami.5b12081.
13. Xiang, H. F.; Wang, H.; Chen, C. H.; Ge, X. W.; Guo, S.; Sun, J. H.; Hu, W. Q. Thermal stability of LiPF6-based electrolyte and effect of contact with various delithiated cathodes of Li-ion batteries. *J Power Sources* 2009, *191* (2), 575-581. DOI: 10.1016/j.jpowsour.2009.02.045.
14. Li, W. D.; Asl, H. Y.; Xie, Q.; Manthiram, A. Collapse of LiNi1-x-yCoxMnyO2 Lattice at Deep Charge Irrespective of Nickel Content in Lithium-Ion Batteries. *J Am Chem Soc* 2019, *141* (13), 5097-5101. DOI: 10.1021/jacs.8b13798.
15. Belharouak, I.; Vissers, D.; Amine, K. Thermal stability of the

Li(Ni0.8Co0.15Al0.05)O−2 cathode in the presence of cell components. *J Electrochem Soc* 2006, *153* (11), A2030−A2035. DOI: 10.1149/1.2336994.

16. Jung, C. H.; Kim, D.; Eum, D.; Kim, K. H.; Choi, J.; Lee, J.; Kim, H. H.; Kang, K.; Hong, S. H. New Insight into Microstructure Engineering of Ni−Rich Layered Oxide Cathode for High Performance Lithium Ion Batteries. *Adv Funct Mater* 2021, *31* (18). DOI: 10.1002/adfm.202010095.
17. Wang, Q. S.; Jiang, L. H.; Yu, Y.; Sun, J. H. Progress of enhancing the safety of lithium ion battery from the electrolyte aspect. *Nano Energy* 2019, *55*, 93−114. DOI: 10.1016/j.nanoen.2018.10.035.
18. Lim, B. B.; Yoon, S. J.; Park, K. J.; Yoon, C. S.; Kim, S. J.; Lee, J. J.; Sun, Y. K. Advanced Concentration Gradient Cathode Material with Two−Slope for High−Energy and Safe Lithium Batteries. *Adv Funct Mater* 2015, *25* (29), 4673−4680. DOI: 10.1002/adfm.201501430.
19. Park, K. J.; Choi, M. J.; Maglia, F.; Kim, S. J.; Kim, K. H.; Yoon, C. S.; Sun, Y. K. High−Capacity Concentration Gradient Li[Ni0.865Co0.120Al0.015]O−2 Cathode for Lithium−Ion Batteries. *Adv Energy Mater* 2018, *8* (19). DOI: 10.1002/aenm.201703612.
20. Bak, S. M.; Hu, E. Y.; Zhou, Y. N.; Yu, X. Q.; Senanayake, S. D.; Cho, S. J.; Kim, K. B.; Chung, K. Y.; Yang, X. Q.; Nam, K. W. Structural Changes and Thermal Stability of Charged LiNixMnyCozO2 Cathode Materials Studied by Combined In Situ Time−Resolved XRD and Mass Spectroscopy. *Acs Appl Mater Inter* 2014, *6* (24), 22594−22601. DOI: 10.1021/am506712c.
21. Wandt, J.; Freiberg, A. T.; Ogrodnik, A.; Gasteiger, H. A. Singlet oxygen evolution from layered transition metal oxide cathode materials and its implications for lithium−ion batteries. *Materials Today* 2018, *21* (8), 825−833.

22. Jung, R.; Metzger, M.; Maglia, F.; Stinner, C.; Gasteiger, H. A. Chemical versus Electrochemical Electrolyte Oxidation on NMC111, NMC622, NMC811, LNMO, and Conductive Carbon. *J Phys Chem Lett* 2017, *8* (19), 4820−4825. DOI: 10.1021/acs.jpclett.7b01927.
23. Li, T. Y.; Yuan, X. Z.; Zhang, L.; Song, D. T.; Shi, K. Y.; Bock, C. Degradation Mechanisms and Mitigation Strategies of Nickel−Rich NMC−Based Lithium−Ion Batteries. *Electrochem Energy R* 2020, *3* (1), 43−80. DOI: 10.1007/s41918−019−00053−3.
24. Hong, J.; Lim, H. D.; Lee, M.; Kim, S. W.; Kim, H.; Oh, S. T.; Chung, G. C.; Kang, K. Critical Role of Oxygen Evolved from Layered Li−Excess Metal Oxides in Lithium Rechargeable Batteries. *Chem Mater* 2012, *24* (14), 2692−2697. DOI: 10.1021/cm3005634.
25. Kim, K.; Ma, H.; Park, S.; Choi, N. S. Electrolyte−Additive−Driven Interfacial Engineering for High−Capacity Electrodes in Lithium−Ion Batteries: Promise and Challenges. *Acs Energy Lett* 2020, *5* (5), 1537−1553. DOI: 10.1021/acsenergylett.0c00468.
26. Kumai, K.; Miyashiro, H.; Kobayashi, Y.; Takei, K.; Ishikawa, R. Gas generation mechanism due to electrolyte decomposition in commercial lithium−ion cell. *J Power Sources* 1999, *81*, 715−719. DOI: 10.1016/S0378−7753(98)00234−1.
27. Zeng, Z. Q.; Wu, B. B.; Xiao, L. F.; Jiang, X. Y.; Chen, Y.; Ai, X. P.; Yang, H. X.; Cao, Y. L. Safer lithium ion batteries based on nonflammable electrolyte. *J Power Sources* 2015, *279*, 6−12. DOI: 10.1016/j.jpowsour.2014.12.150.
28. Zhou, D. Y.; Li, W. S.; Tan, C. L.; Zuo, X. X.; Huang, Y. J. Cresyl diphenyl phosphate as flame retardant additive for lithium−ion batteries. *J Power Sources* 2008, *184* (2), 589−592. DOI: 10.1016/j.jpowsour.2008.03.008.
29. Cho, W.; Kim, S. M.; Lee, K. W.; Song, J. H.; Jo, Y. N.; Yim, T.; Kim, H.; Kim, J. S.; Kim, Y. J. Investigation of new manganese

orthophosphate Mn-3(PO4)(2) coating for nickel-rich LiNi0.6Co0.2Mn0.2O2 cathode and improvement of its thermal properties. *Electrochim Acta* 2016, *198*, 77-83. DOI: 10.1016/j.electacta.2016.03.079.

30. Lu, X. X.; Zhang, N. X.; Jahn, M.; Pfleging, W.; Seifert, H. J. Improved Capacity Retention of SiO2-Coated LiNi0.6Mn0.2Co0.2O2 Cathode Material for Lithium-Ion Batteries. *Appl Sci-Basel* 2019, *9* (18). DOI: 10.3390/app9183671.
31. Liu, K.; Liu, W.; Qiu, Y. C.; Kong, B. A.; Sun, Y. M.; Chen, Z.; Zhuo, D.; Lin, D. C.; Cui, Y. Electrospun core-shell microfiber separator with thermal-triggered flame-retardant properties for lithium-ion batteries. *Sci Adv* 2017, *3* (1). DOI: 10.1126/sciadv.1601978.
32. Kim, C. K.; Shin, D. S.; Kim, K. E.; Shin, K.; Woo, J. J.; Kim, S.; Hong, S. Y.; Choi, N. S. Fluorinated Hyperbranched Cyclotriphosphazene Simultaneously Enhances the Safety and Electrochemical Performance of High-Voltage Lithium-Ion Batteries. *Chemelectrochem* 2016, *3* (6), 913-921. DOI: 10.1002/celc.201600025.
33. Korobeinichev, O. P.; Ilyin, S. B.; Bolshova, T. A.; Shvartsberg, V. M.; Chernov, A. A. The chemistry of the destruction of organophosphorus compounds in flames - III: The destruction of DMMP and TMP in a flame of hydrogen and oxygen. *Combust Flame* 2000, *121* (4), 593-609. DOI: 10.1016/S0010-2180(99)00171-6.
34. Allcock, H. R.; Taylor, J. P. Phosphorylation of phosphazenes and its effects on thermal properties and fire retardant behavior. *Polym Eng Sci* 2000, *40* (5), 1177-1189. DOI: 10.1002/pen.11245.
35. Kim, S. Y.; Park, C. S.; Hosseini, S.; Lampert, J.; Kim, Y. J.; Nazar, L. F. Inhibiting Oxygen Release from Li-rich, Mn-rich Layered Oxides at the Surface with a Solution Processable Oxygen

Scavenger Polymer. *Adv Energy Mater* 2021, *11* (30). DOI: 10.1002/aenm.202100552.

국문 초록

고안정성 리튬이온전지를 위한 포스포노 화합물을 이용한 $LiNi_{0.945}Co_{0.04}Al_{0.015}O_2$의 표면 개질

정해민
서울대학교 대학원
화학생물공학부

고-니켈계 리튬 전이금속 산화물 양극재는 높은 가역 용량으로 인해 차세대 양극재로 주목받고 있다. 이때 양극재의 가역 용량은 니켈의 함량이 증가함에 따라 증가하는데, 동시에 구조적 안정성도 감소한다. 리튬 전이금속 산화물 양극재의 구조적 불안정성은 양극재 격자 구조의 산소가 산소 라디칼의 형태로 방출되게 한다. 산소의 방출은 양극 성능의 저하를 가져올 뿐 아니라, 열폭주 현상을 유발하여 배터리의 안정성을 악화시킨다.

본 연구에서, 라디칼을 포획하는 고-니켈계 양극재의 표면을 PBA를 통한 표면개질을 통해 양극재로부터 방출되는 산소 라디칼의 방출을 막아 양극재의 열안정성을 높이는 방법을 제시하였다. 이를 위해 라디칼을 포획하는 코팅층은 자유 라디칼을 포획하는 특성이 있는 인을 포함하는 포스포노 벤조익 액시드를 이용한 표면 공정을 통해 도입하였다. 이 공정을 통해 열안정성을 개선하고 전해질 분해와 가스 생성을 줄이고, 코팅을 하지 않은 것과 비교해 비슷한 전기화학 특성을 유지했다.

키워드 : 리튬 이온 전지, 고-니켈계 양극 소재, 라디칼 포획, 산소 방출, 배터리 안전

학번 : 2020-29311